PNAS RESEARCH ARTICLE | APPLIED PHYSICAL SCIENCES

Experimental observations of marginal criticality in granular materials

Yinqiao Wang[a,b], Jin Shang[a], Yuliang Jin[c,d,e], and Jie Zhang[a,f,1]

Edited by Giorgio Parisi, Universita degli Studi di Roma La Sapienza, Rome, Italy; received March 20, 2022; accepted April 12, 2022

Two drastically different theories predict the marginal criticality of jamming. The full replica symmetry breaking (fullRSB) theory predicts the power-law distributions of weak contact forces and small interparticle gaps in infinite-dimensional hard-sphere glass, with two nontrivial exponents $\theta_f = 0.42311\ldots$ and $\gamma = 0.41269\ldots$, respectively. Independently, the marginal mechanical stability (MMS) analysis predicts that the isostatic random packings of hard frictionless spheres under external stress are marginally stable and provides inequality relationships for the exponents of the weak-force and interparticle-gap distributions. Here, we measure precisely contact forces and particle positions in isotropic jammed bidisperse photoelastic disks and find the clear power-law distributions of weak forces and small interparticle gaps, with both exponents $\theta_f = 0.44(2)$ and $\gamma = 0.43(3)$ in an excellent agreement with the fullRSB theory. As the jammed packing subject to area-conserved cyclic pure shear approaches the yielding point, the two exponents change substantially from those of the isotropic case, but they still satisfy the scaling relationship provided by the MMS argument. Our results provide strong experimental evidence for the robustness of the infinite-dimensional theory and the MMS analysis in real-world amorphous materials.

jamming | glass | marginal stability

A liquid undergoes a glass transition upon fast quench (1, 2), whereas in the athermal situation, a flowing granular material undergoes a jamming transition subjected to compression (3–5) or shear (6), with subtle structural changes while gaining rigidity. The deep connection between the two transitions has been thought for a long time (3). Two independent theories were developed for the marginal criticality of hard spheres near jamming: One is the first-principle replica theory of hard-sphere glass in infinite dimensions (2, 7), and the other is the marginal mechanical stability (MMS) analysis for isostatic random hard-sphere (or disk) packings in finite dimensions (8–11).

The first-principle theoretical description of amorphous materials is extremely challenging (12). The recent full replica symmetry breaking (fullRSB) theory of the hard-sphere glass in infinite dimensions (2, 7, 13) unifies the glass transition and the jamming transition within the statistical mechanics framework, echoing Liu and Nagel's (3) seminal proposal made years ago. Moreover, this theory points out a Gardner transition (2, 7) within the glass phase similarly existing in the spin glass (14). The fullRSB theory (2, 7) predicts that when a stable glass undergoes a Gardner transition, either by compression or cooling, the metastable basins in the free-energy landscape break into a fractal hierarchy of subbasins, forming a marginal phase. For hard spheres, the jamming transition manifested by the divergence of pressure happens deeply inside the marginal phase. Specifically, the fullRSB solution delivers three nontrivial power-law exponents of κ, γ, and θ_f characterizing jamming, including the cage size Δ versus the pressure p, $\Delta \sim p^{-\kappa}$ with $\kappa = 1.41574\ldots$, the distribution of small interparticle gaps $P(h) \sim h^{-\gamma}$ with $\gamma = 0.41269\ldots$, and the distribution of weak contact forces $P(f) \sim f^{\theta_f}$ with $\theta_f = 0.42311\ldots$ (2, 7).

Indeed, before the fullRSB theory (2, 7), the relationships between these three critical exponents were already predicted by the independently developed MMS analysis (8–11). Thus, the jamming criticality results from the remarkable convergence of two completely independent lines of research associated with two types of marginal stability (15, 16). The first type refers to the (free-energy) landscape marginal stability of the Gardner phase (2, 7), which resembles that of spin glass. The second type (8, 10, 11) closely related to isostaticity refers to the MMS of jammed packings, as introduced in the jamming field (3–5, 8, 10, 17, 18). While the low-energy excitation of the Gardner phase is presumably system-wide extended in the limit of infinite dimensions (19), both extended and localized modes may exist in low dimensions. Besides the weak-force exponent θ_e, satisfying $\theta_e = 1/\gamma - 2$, which is associated with the extended excitation and coincides with the θ_f in infinite dimensions, the MMS also includes an extra exponent θ_l associated with the localized excitation, satisfying $\theta_l = 1 - 2\gamma$ (10).

Significance

Amorphous materials, such as grains, foams, colloids, and glasses, are ubiquitous in nature and our daily life. They can undergo glass transitions or jamming transitions to obtain rigidity either by fast quench or compression, but show subtle changes in the structures compared to the liquid states or liquid-like states. Recent progress on the first-principle replica theory unifies the glass transition and the jamming transition and points out the marginal phase with fractal free-energy landscape within the stable glass phase. Independently, marginal stability analysis predicts the relations between the exponents of the marginal phase. Here, we perform experiments with photoelastic disks and provide direct evidence of these theories in real-world amorphous materials.

Author affiliations: [a]School of Physics and Astronomy, Shanghai Jiao Tong University, 200240 Shanghai, China; [b]Research Center for Advanced Science and Technology, University of Tokyo, Tokyo 153-8505, Japan; [c]Institute of Theoretical Physics, Chinese Academy of Sciences, Beijing 100190, China; [d]School of Physical Sciences, University of Chinese Academy of Sciences, Beijing 100049, China; [e]Wenzhou Institute, University of Chinese Academy of Sciences, Wenzhou 325000, China; and [f]Institute of Natural Sciences, Shanghai Jiao Tong University, 200240 Shanghai, China

Author contributions: Y.W. and J.Z. designed research; Y.W. and J.S. performed research; Y.W. and J.S. analyzed data; and Y.W., J.S., Y.J., and J.Z. wrote the paper.

The authors declare no competing interest.

This article is a PNAS Direct Submission.

[1]To whom correspondence may be addressed. Email: jiezhang2012@sjtu.edu.cn.

This article contains supporting information online at https://www.pnas.org/lookup/suppl/doi:10.1073/pnas.2204879119/-/DCSupplemental.

Published May 24, 2022.

Since the upper critical dimension of jamming is conjectured to be two (17, 20), the robustness of the fullRSB theory needs to be verified in two or three dimensions, in particular, in experiments. In the last decade, numerous simulations (2, 9, 10, 20–24) have been performed. The exponent κ, closely related to the dynamical information of caging, has been verified in simulations of the dimension $d = 3 - 8$ (2). Nevertheless, the two exponents γ and θ_f can be directly obtained from a static packing. The exponent $\gamma \approx 0.4$ of the interparticle gaps is known to be constant in all dimensions, regardless of preparation protocols (9, 21, 25–27), except $\gamma \approx 0.5$ (9, 28), when including rattlers (9). However, the exponent θ_f of the weak contact forces is more sensitive to the dimension and preparation protocols, and its value has been reported within the range of 0 to 0.45 (9, 10, 19, 21–23, 25, 29). Recently, the solution of this controversy was proposed by Charbonneau et al. (19): If localized buckling excitation is removed, the exponent of the weak-force distributions coincides with the infinite-dimension solution $\theta_f = 0.42311$ in $d = 2 - 4$.

The experimental verification of the marginal criticality of jamming is rare. Indirect characterizations of the Gardner phase through particle dynamics has been performed in model glass systems, such as the cage separation upon compression in vibrated granular matter (30, 31) and the logarithmic growth of the mean square displacement in colloidal glass (32). Yet, direct quantitative verification of the critical exponents of the fullRSB theory (2, 7) and the relationship between the weak-force exponents and the small-gap exponent (8, 10, 11) in experiments are still lacking.

Results

To measure interparticle contact forces and particle positions, we perform a two-dimensional experiment with bidisperse photoelastic disks of 1,355 large disks and 2,710 small disks, whose diameters are 1.4 cm and 1.0 cm, respectively. Experimental details are described in *Materials and Methods*.

Criticality of Weak Contact Forces. A typical experimental stress image is plotted in Fig. 1*A*, and the corresponding force network is plotted in Fig. 1*B*. To quantify the heterogeneity of the force network, plenty of works (33–36) have focused on the tail of force distribution, which is closely related to the statistical framework of granular materials. Nevertheless, marginal criticality of jammed packings is often related to the distribution of weak contact forces (11), i.e., the contact forces smaller than the mean value. From the mechanical stability perspective, the weak forces are most likely to open under external perturbations to destabilize the packing. Alternatively, from the perspective of the hierarchical free-energy landscape, the weak-force distributions reflect the structure of the hierarchy basins in the free-energy landscape of the packing. Fig. 1*C* shows the probability distributions of contact forces $P(f)$ for different pressure levels on log–log scale. Here, $P(f)$, as well as $g(h)$ mentioned below, are ensemble averaged over 30 jammed configurations. Limited by the measurement resolution—that is, the minimum force $f \approx 0.05$ N can be accurately measured—we cannot observe clear scalings of weak-force distributions at low pressure.

Subjected to isotropic compression, the global pressure of the jammed packing increases, and the range of reliable scaling becomes sufficiently large—that is, $f \in [0.05, 0.6 \times \langle f \rangle]$, with $\langle f \rangle$ referring to the mean force. By fitting with a power law, the exponent θ_f at different pressure can be extracted and is plotted in Fig. 1 *C*, *Inset*. We can see that the exponent θ_f saturates for large pressures, whose value shows an excellent agreement with that of the fullRSB theory (2, 7). The critical exponent $\theta_f = 0.42311$ is indicated as the dashed line both in the main panel and *Inset* of Fig. 1*C*.

Note that, upon compression, even as the pressure and the contact number of the overjammed packings exceed the values at the jamming point, the associated packings are still close to the MMS, which is due to the excess contact number required to stabilize the packing due to the external pressure (17, 37). In other words, a small increment of pressure tends to destabilize the packing of the fixed contact number, and, hence, the accompanying increase of the contact number would stabilize the packing at the new pressure level. Further, the excess contact number reduces the fraction of bucklers significantly (19), which explains that the measured exponent $\theta_f = 0.44(2)$ in our case is close to the $\theta_e = 0.42$, but deviates substantially from the $\theta_l = 0.17$ due to the bucklers (19).

Criticality of Small Interparticle Gaps. While the opening of contacts bearing weak forces destabilizes the packing, the nearly touched contacts can close the gaps to form new contacts to stabilize the packing. For monodisperse packings, the distribution

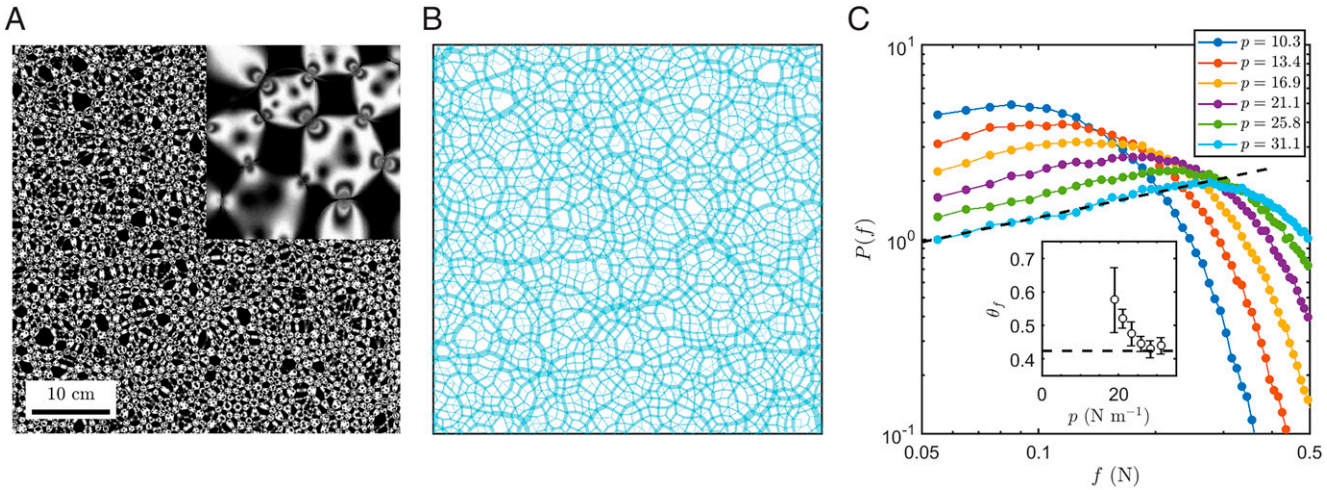

Fig. 1. Interparticle contact forces in compression jammed packings. (*A*) A typical experimental stress image of photoelastic disks visualized by two matched circular polarizers, in which a small portion of the image is enlarged. (*B*) The corresponding force network is plotted, in which the thicknesses of bond are proportional to the magnitudes of the measured contact forces. (*C*) The probability density distributions of contact forces $P(f)$ for isotropically jammed packings at different pressure levels. *C*, *Inset* shows the fitted power-law exponent θ_f of $P(f)$ versus pressure levels, and error bars represent SDs of the fitted coefficients. The black dashed lines in the main panel and *Inset* represent a power law with an exponent $\theta_f = 0.42311$, which is given by the fullRSB theory.

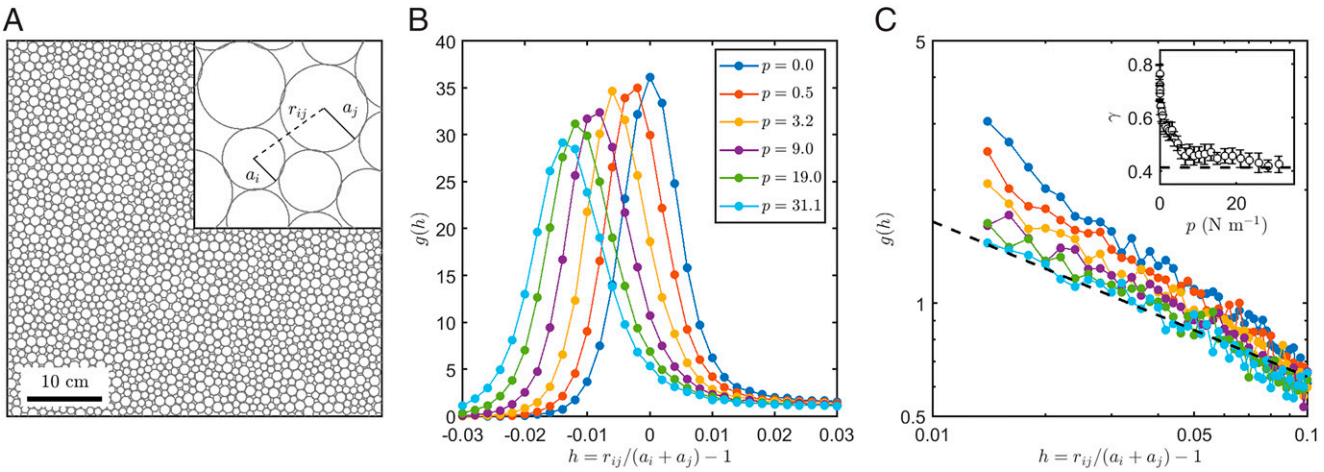

Fig. 2. Interparticle gaps in compression jammed packings. (*A*) A snapshot of a typical bidisperse photoelastic disks packing. (*B*) Radial distribution functions $g(h)$ of the interparticle gap h at different pressure levels. Here, $h = r_{ij}/(a_i + a_j) - 1$ is the dimensionless interparticle gap between particle i and particle j, in which a_i and a_j are the radii of particles i and j, respectively, and r_{ij} is the distance between particles i and j. (*C*) $g(h)$ plotted on a log–log scale. *C*, *Inset* shows the power-law exponent γ of $g(h)$ fitted in the range [0.012, 0.05] versus the pressure levels. The black dashed lines in the main panel and *Inset* represent a power law with an exponent $\gamma = 0.41269$, which is given by the fullRSB theory.

of small gaps can be directly given by the radial distribution function $g(r)$. Due to the bidisperse characteristic in our experiments, the first peak of $g(r)$ will split into three peaks. To avoid the effects of bidispersity, we define the dimensionless interparticle gaps as $h = r_{ij}/(a_i + a_j) - 1$, where r_{ij} is the distance between two neighboring particles i and j, and a_i and a_j are the radii of the two particles, respectively, as shown in Fig. 2*A*. Finally, we obtain the distributions of dimensionless interparticle gaps $g(h)$, as shown in Fig. 2 *B* and *C*.

For sphere packings near the jamming transition, $g(h)$ is a delta function at $h = 0$ followed by a power-law decay $g(h) \propto h^{-\gamma}$ (25, 28). However, the delta function often smears out due to the uncertainty of particle positions in experiments, as shown in Fig. 2*B*. The width of the Gaussian-like peak at $h = 0$ is around 0.01, which indicates that the uncertainty of the particle detection is around a half-pixel. Even if the small interparticle gaps had a power-law scaling, it would be hidden by the Gaussian-like peak near $h = 0$. For soft sphere packings, the peak of $g(h)$ shifts down upon compression, as shown in Fig. 2*B*. Therefore, applying compression on the packings helps to disentangle the Gaussian-like peak and the scaling of positive interparticle gaps with $h > 0$. In Fig. 2*C*, we plot $g(h)$ on log–log scale and find an increasingly clear power-law scaling as pressure increases. As the very small gaps are interfered with by the accuracy of particle positions, and, meanwhile, the critical scaling may break down for large gaps, we fit the $g(h)$ in the range $h \in [0.012, 0.05]$ to the power law. The fitted exponents are shown in Fig. 2 *C*, *Inset*. Similar to the exponent θ_f of weak forces, the exponent γ is also in good agreement with the fullRSB solution, indicated by the dashed lines in Fig. 2*C*. Note that the fraction of rattlers is around 0.8% in the overjammed packings and, thus, negligible.

Nonuniversal Criticality in Sheared Packings with Friction. In simulations of hard-sphere glass, the packing fraction of jamming point ϕ_J depends on the parent liquid state and the preparation protocol, which results in the jamming line (2, 27). Specifically, a denser parent liquid produces a denser jammed packing (2), and applying shear further expands the phase space of jammed states (27). Nevertheless, the marginal critical scalings associated with jamming are universal, regardless of the path to jam, and the associated exponents, including $\gamma \approx 0.4$ (27, 38), $\theta_e \approx 0.42$ and $\theta_l \approx 0.17$ (38), remain unchanged. Next, we will show, however, that for jammed frictional particles, the situation becomes different.

Fig. 3*A* shows a typical force network of the jammed packings prepared under the steady-state cyclic pure shear, in which the global stress ratio μ (see *Materials and Methods* for details) is around 0.41. Both the weak-force distributions $P(f)$ and the small-interparticle-gap distributions $g(h)$ depart obviously from the infinite-dimensional solution, as shown in Fig. 3 *B* and *C*. This might explain the relatively large range of the exponent $\gamma \in [0.25, 0.75]$ reported in colloidal (39) and granular experiments (40) under gravity. While $P(f)$ typically shows a peak around the mean contact force for isotropically jammed packings, as shown in Fig. 1 and also in literature (29, 33, 34), the peaks disappear here in Fig. 3: For jammed packings subject to the steady-state cyclic pure shear, within our contact-force resolution, $P(f)$ increase monotonically as f decreases.

Remarkably, even both the weak-forces exponent θ_f and the small-gaps exponent γ deviate substantially from those of the infinite-dimensional solution, they still satisfy the relationship predicted by the MMS analysis (8–11). Here, the global stress ratio $\mu = 0.41$ of the jammed packings subject to the steady-state cyclic pure shear is close to the yielding point. Fig. 3*C* shows that the exponent γ of small gaps is around 0.56. According to the theory (8, 10, 11), the exponent $\gamma = 0.56$ derives the two weak-force exponents $\theta_l = 1 - 2\gamma = -0.12$ and $\theta_e = 2 - 1/\gamma = -0.21$, which then determine the weak-force exponent θ_f according to the relationship $\theta_f = \min(\theta_l, \theta_e) = \theta_e = -0.21$. As shown in Fig. 3*B*, the $P(f)$ of the packing $\mu = 0.41$ is very close to the power-law scaling with an exponent $\theta_f = -0.21$, plotted as the red dotted line, which indicates that the bound between θ_f and γ is marginally satisfied. Moreover, as estimated from γ, the fact that $\theta_e < \theta_l$ suggests that the extended excitation becomes dominant in the weak-force region for jammed packings subject to the steady-state cyclic pure shear near yielding. Note that the systematic evaluation of θ_f deteriorates rapidly for $\mu < 0.41$ since the pressure drops with μ, and, hence, the power-law regime narrows substantially.

Discussion

We have experimentally investigated the marginal criticality in jammed bidisperse photoelastic disks.

First, we have measured the power-law exponents of the weak-force distributions and the small-interparticle-gap distributions in

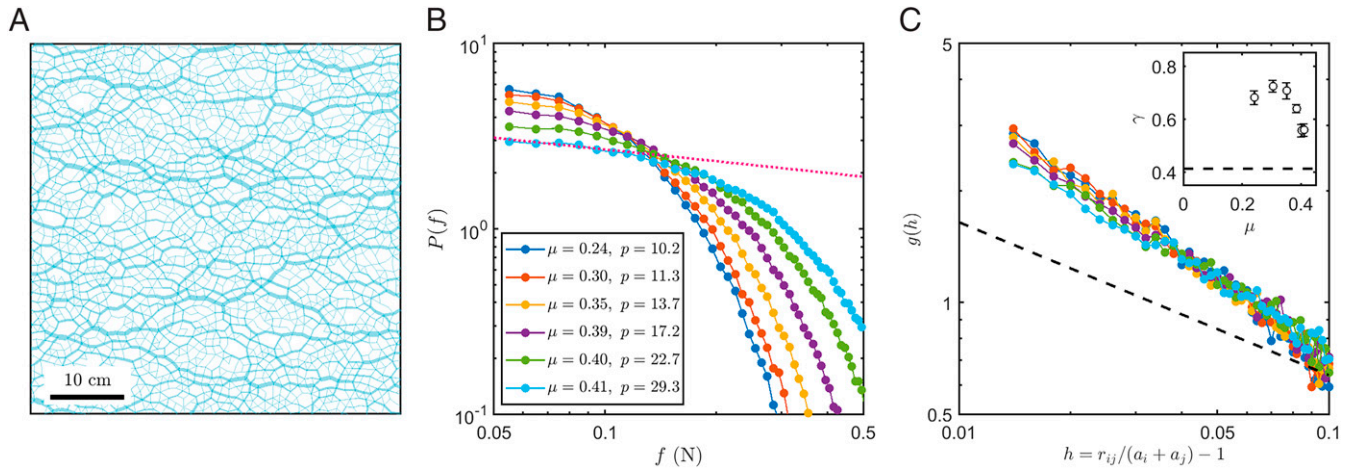

Fig. 3. Interparticle forces and gaps in jammed packings subject to cyclic shear. (*A*) A typical force network for jammed packings subject to cyclic pure shear. (*B* and *C*) Distributions of interparticle forces $P(f)$ (*B*) and distributions of interparticle gaps $g(h)$ (*C*) for jammed packings with different global stress ratios μ. The red dotted line represents the power law with an exponent $\theta_f = -0.21$, which is derived from the exponent $\gamma = 0.56$ and the scaling relationship given by the MMS analysis. The black dashed lines in *C* represent a power law with an exponent $\gamma = 0.41269$, as a guide for the eye.

the isotropic jammed packings. As the global pressure increases, the interval of the weak forces (i.e., $f < \langle f \rangle$) above the minimum force resolution increases significantly, and, meanwhile, the localized excitation is suppressed. We thus can obtain a reliable measurement of the weak-force exponent associated with extended excitation, i.e., $\theta_f = \theta_e = 0.44(2)$, and the small-interparticle-gap exponent $\gamma = 0.43(3)$, both of which agree extremely well with those of the fullRSB solution (2, 7).

Next, we investigate the two exponents in the jammed packings produced in the steady-state cyclic pure shear. We find that both exponents of θ_f and γ deviate substantially from those of the isotropic case; especially when the stress ratio μ approaches the yielding point, the accompanied pressure value increases significantly due to shear-induced dilation that creates reasonably wide ranges of power-law scaling. Remarkably, the two exponents still satisfy the relationship predicted by the MMS (8, 10, 11). Furthermore, the extended modes dominate over the low-energy excitation based on the estimation from γ, implying that the avalanche dynamics of granular materials shall percolate the whole system near the yielding point.

Note that the interparticle friction in our system is beyond the present scope of the fullRSB theory (2, 7). We believe that friction expands the phase space of the jammed states significantly compared with that of the frictionless spheres or disks. Recall that to create the isotropic jammed packings, we first prepare an initial stress-free packing with the packing fraction $\phi = 83.4\%$, close to the two-dimensional jamming point of frictionless particles $\phi_J \approx 84\%$ (4), and then we apply constant vibrations at the bottom plate to eliminate the base friction. Adopting this preparation protocol allows us to generate the almost perfectly uniform and isotropic jammed packings (41, 42), from which we obtain the good statistics of the contact forces and interparticle gaps that are consistent with the prediction of frictionless hard spheres (2, 7). To create the jammed packings upon the steady-state pure shear of conserved area, we believe that the interparticle friction plays an important role in selecting the jammed states in the expanded phase space, which, therefore, changes the exponents of $P(f)$ and $g(h)$.

It has been reported that the Gardner phase is not necessarily universally observed (43, 44) in finite-dimensional glasses far away from jamming. The fact that the jamming criticalities are observed in low dimensions might be due to the emergence of hyperuniformity (45–48) in jammed packings, which may suppress the fluctuations in finite-dimensional systems. Meanwhile, a clear theoretical basis for the superuniversality of jamming is still lacking (5, 16, 20, 49).

In the future, the connection between these critical scalings of microstructures and the rheological dynamics of amorphous solids needs to be studied. In addition, the effects of particle shape on the microstructures of interparticle gaps and contact forces (50) can be explored by using the photoelastic ellipses (33).

Materials and Methods

Experimental Setup. The layer of particles is placed on a horizontal glass plate and is laterally confined by two pairs of walls, forming a rectangle. The two pairs of walls can move inward simultaneously to apply isotropic compression, or one pair moves inward and the other pair moves outward to apply area-conserved pure shear. To eliminate the friction between the particle layer and the glass plate, we attach eight mini vibrators below the glass plate. At the top, an array of 2×2 high-resolution (100 pixels/cm) cameras are aligned and synchronized. A pair of matched circular polarizers are inserted above and below the particle layer. The top polarizer is right below the array of cameras and can be moved horizontally in and out under the control of a motor. A uniform green light box is mounted at the bottom.

Preparation Protocols of Jammed Packings Subject to Isotropic Compression. Packings at different pressure levels subject to isotropic compression are prepared as follows. We first prepare a stress-free random and homogeneous particle configuration with the packing fraction $\phi = 83.4\%$ (the ratio between the area of disks and that of the rectangle) near the jamming point $\phi_J \approx 84.0\%$ of frictionless particles. To achieve this goal, we start from a random loose initial configuration by filling a random mixture of bidisperse photoelastic disks within the rectangle. When applying isotropic compression to increase the ϕ, we constantly apply manual agitation within the photoelastic disks to remove any transient force chains and, meanwhile, turn on the mini vibrators to eliminate the base friction. After the stress-free random initial packing with $\phi = 83.4\%$ is prepared, we stop manual agitation for any further isotropic compression. Next, we apply isotropic compression in incremental steps to obtain packings at a sequence of incremental pressure levels with maximum packing fraction $\phi = 86.2\%$. During this process, the mini vibrators are synchronized with the movement of the four walls, such that they are turned on when the walls move and are turned off when the walls pause after an incremental step. The force chains of isotropically jammed packings are homogeneous and isotropic. An example of an original stress image and the associated force-network image are shown in Fig. 1 *A* and *B*. Note that we can generate an ensemble of sets of isotropically jammed packings by applying the above protocol repetitively.

Preparation Protocols of Jammed Packings Subject to Pure Shear. Packings of different pressure levels subject to area-conserved pure shear are prepared as follows. We first follow the protocol of preparing a weakly jammed packing subject to isotropic compression with the packing fraction $\phi = 85.0\%$. We then apply pure shear to this packing to drive the system into steady states, in which the curve of the global stress ratio $\mu \equiv \tau/p$ versus the strain of every shear cycle remains fixed. Here, the global stress ratio μ refers to the ratio between the global shear stress τ and the pressure p of the system. The strain ϵ of every shear cycle is in between $\epsilon_{min} = -2.8\%$ and $\epsilon_{max} = 2.8\%$. We apply pure shear in incremental steps to cover a sequence of strains within $\epsilon_{min} \leq \epsilon \leq \epsilon_{max}$. During this process, the mini vibrators are synchronized with the movement of the four walls, such that they are turned on when the walls move and are turned off when the walls pause after an incremental step. Since there is shear-induced dilation in area-conserved cyclic pure shear, the pressure p of the system is not a constant, and, hence, we obtain a sequence packings of different μ and p subject to cyclic pure shear. Note that we can similarly generate an ensemble of sets of cyclically sheared jammed packings by applying the above protocol repetitively.

Particle Detection and Contact Force Measurements. For each step of compression or shear, we record one stress image, as shown in Fig. 1*A*, and one normal image, depending on whether the top polarizer is inserted or removed. With the normal image, we use the Hough transform algorithm to detect the positions of particles with subpixel resolutions. We can then obtain interparticle contacts with the criterion of $r_{ij} < (1+\delta)(a_i + a_j)$. Here, r_{ij} is the distance between particle i and particle j, a_i and a_j are the radii of particles, and δ is set as 0.05 to avoid the missing of force-bearing contacts. Note that although this value of δ may include a few false contacts, it, however, will not affect the results presented in this paper since the measured contact forces of those false contacts are smaller than 0.05 N. With the stress image and the positions of particles and contacts, we can solve the contact force vectors using a force-inverse algorithm, which generates a computed stress image based on an initial guess of contact forces, and then iterate to minimize the difference between the experimental and computed stress images. The relative error of contact force measurement is less than 5% for the typical force magnitude; when $f < 0.05$ N, measurements are often interfered with by the inhomogeneity of background illuminations and limited by the image resolution. Our final remark is regarding the mini vibrators: Applying vibration using mini vibrators efficiently eliminates the base friction, but this method will not produce noticeable effects in the relaxation of the stress images. For a jammed packing, we turn on the mini vibrators for a considerably long time, and we compare the stress images before and after and see no noticeable changes.

Data Availability. All study data are included in the article.

ACKNOWLEDGMENTS. Y.W., J.S., and J.Z. acknowledge support from National Natural Science Foundation of China (NSFC) Grants 11974238 and 11774221 and from Innovation Program of Shanghai Municipal Education Commission Grant 2021-01-07-00-02-E00138. Y.W., J.S., and J.Z. also acknowledge support from the Student Innovation Center of Shanghai Jiao Tong University. Y.W. acknowledges support from Shanghai Jiao Tong University via the scholarship for outstanding Ph.D. graduates. Y.J. acknowledges support from NSFC Grants 11974361, 12161141007, 11935002, and 12047503; from the Key Research Program of Frontier Sciences, Chinese Academy of Sciences, Grant ZDBS-LY-7017; and from the Key Research Program of the Chinese Academy of Sciences Grant XDPB15.

1. G. Parisi, F. Zamponi, Mean-field theory of hard sphere glasses and jamming. *Rev. Mod. Phys.* **82**, 789–845 (2010).
2. P. Charbonneau, J. Kurchan, G. Parisi, P. Urbani, F. Zamponi, Fractal free energy landscapes in structural glasses. *Nat. Commun.* **5**, 3725 (2014).
3. A. J. Liu, S. R. Nagel, Nonlinear dynamics: Jamming is not just cool any more. *Nature* **396**, 21–22 (1998).
4. C. S. O'Hern, L. E. Silbert, A. J. Liu, S. R. Nagel, Jamming at zero temperature and zero applied stress: The epitome of disorder. *Phys. Rev. E Stat. Nonlin. Soft Matter Phys.* **68**, 011306 (2003).
5. A. J. Liu, S. R. Nagel, The jamming transition and the marginally jammed solid. *Annu. Rev. Condens. Matter Phys.* **1**, 347–369 (2010).
6. D. Bi, J. Zhang, B. Chakraborty, R. P. Behringer, Jamming by shear. *Nature* **480**, 355–358 (2011).
7. P. Charbonneau, J. Kurchan, G. Parisi, P. Urbani, F. Zamponi, Exact theory of dense amorphous hard spheres in high dimension. III. The full replica symmetry breaking solution. *J. Stat. Mech. Theory Exp.* **2014**, P10009 (2014).
8. M. Wyart, Marginal stability constrains force and pair distributions at random close packing. *Phys. Rev. Lett.* **109**, 125502 (2012).
9. E. Lerner, G. Düring, M. Wyart, Low-energy non-linear excitations in sphere packings. *Soft Matter* **9**, 8252–8263 (2013).
10. E. DeGiuli, E. Lerner, C. Brito, M. Wyart, Force distribution affects vibrational properties in hard-sphere glasses. *Proc. Natl. Acad. Sci. U.S.A.* **111**, 17054–17059 (2014).
11. M. Müller, M. Wyart, Marginal stability in structural, spin, and electron glasses. *Annu. Rev. Condens. Matter Phys.* **6**, 177–200 (2015).
12. P. Charbonneau, J. Kurchan, G. Parisi, P. Urbani, F. Zamponi, Glass and jamming transitions: From exact results to finite-dimensional descriptions. *Annu. Rev. Condens. Matter Phys.* **8**, 265–288 (2017).
13. G. Parisi, P. Urbani, F. Zamponi, *Theory of Simple Glasses: Exact Solutions in Infinite Dimensions* (Cambridge University Press, Cambridge, UK, 2020).
14. E. Gardner, Spin glasses with p-spin interactions. *Nucl. Phys. B* **257**, 747–765 (1985).
15. S. Franz, G. Parisi, P. Urbani, F. Zamponi, Universal spectrum of normal modes in low-temperature glasses. *Proc. Natl. Acad. Sci. U.S.A.* **112**, 14539–14544 (2015).
16. L. Berthier *et al.*, Gardner physics in amorphous solids and beyond. *J. Chem. Phys.* **151**, 010901 (2019).
17. M. Wyart, L. E. Silbert, S. R. Nagel, T. A. Witten, Effects of compression on the vibrational modes of marginally jammed solids. *Phys. Rev. E Stat. Nonlin. Soft Matter Phys.* **72**, 051306 (2005).
18. A. Zaccone, E. Scossa-Romano, Approximate analytical description of the nonaffine response of amorphous solids. *Phys. Rev. B Condens. Matter Mater. Phys.* **83**, 184205 (2011).
19. P. Charbonneau, E. I. Corwin, G. Parisi, F. Zamponi, Jamming criticality revealed by removing localized buckling excitations. *Phys. Rev. Lett.* **114**, 125504 (2015).
20. C. P. Goodrich, A. J. Liu, S. R. Nagel, Finite-size scaling at the jamming transition. *Phys. Rev. Lett.* **109**, 095704 (2012).
21. P. Charbonneau, E. I. Corwin, G. Parisi, F. Zamponi, Universal microstructure and mechanical stability of jammed packings. *Phys. Rev. Lett.* **109**, 205501 (2012).
22. E. Lerner, G. Düring, M. Wyart, Toward a microscopic description of flow near the jamming threshold. *EPL (Europhys. Lett.)* **99**, 58003 (2012).
23. Y. Kallus, Scaling collapse at the jamming transition. *Phys. Rev. E* **93**, 012902 (2016).
24. P. Charbonneau *et al.*, Finite-size effects in the microscopic critical properties of jammed configurations: A comprehensive study of the effects of different types of disorder. *Phys. Rev. E* **104**, 014102 (2021).
25. A. Donev, S. Torquato, F. H. Stillinger, Pair correlation function characteristics of nearly jammed disordered and ordered hard-sphere packings. *Phys. Rev. E Stat. Nonlin. Soft Matter Phys.* **71**, 011105 (2005).
26. M. Skoge, A. Donev, F. H. Stillinger, S. Torquato, Packing hyperspheres in high-dimensional Euclidean spaces. *Phys. Rev. E Stat. Nonlin. Soft Matter Phys.* **74**, 041127 (2006).
27. Y. Jin, H. Yoshino, A jamming plane of sphere packings. *Proc. Natl. Acad. Sci. U.S.A.* **118**, e2021794118 (2021).
28. L. E. Silbert, A. J. Liu, S. R. Nagel, Structural signatures of the unjamming transition at zero temperature. *Phys. Rev. E Stat. Nonlin. Soft Matter Phys.* **73**, 041304 (2006).
29. C. S. O'Hern, S. A. Langer, A. J. Liu, S. R. Nagel, Random packings of frictionless particles. *Phys. Rev. Lett.* **88**, 075507 (2002).
30. A. Seguin, O. Dauchot, Experimental evidence of the Gardner phase in a granular glass. *Phys. Rev. Lett.* **117**, 228001 (2016).
31. H. Xiao, A. J. Liu, D. J. Durian, Probing the Gardner transition in an active quasi-thermal pressure-controlled granular system. arXiv [Preprint] (2021). https://arxiv.org/abs/2111.03921. Accessed 6 November 2021.
32. A. P. Hammond, E. I. Corwin, Experimental observation of the marginal glass phase in a colloidal glass. *Proc. Natl. Acad. Sci. U.S.A.* **117**, 5714–5718 (2020).
33. Y. Wang, J. Shang, Y. Wang, J. Zhang, Contact force measurements and local anisotropy in ellipses and disks. *Phys. Rev. Res.* **3**, 043053 (2021).
34. T. S. Majmudar, R. P. Behringer, Contact force measurements and stress-induced anisotropy in granular materials. *Nature* **435**, 1079–1082 (2005).
35. C. H. Liu *et al.*, Force fluctuations in bead packs. *Science* **269**, 513–515 (1995).
36. B. P. Tighe, J. H. Snoeijer, T. J. Vlugt, M. van Hecke, The force network ensemble for granular packings. *Soft Matter* **6**, 2908–2917 (2010).
37. E. DeGiuli, A. Laversanne-Finot, G. Düring, E. Lerner, M. Wyart, Effects of coordination and pressure on sound attenuation, boson peak and elasticity in amorphous solids. *Soft Matter* **10**, 5628–5644 (2014).
38. V. Babu, S. Sastry, Criticality and marginal stability of the shear jamming transition of frictionless soft spheres. *Phys. Rev. E* **105**, L042901 (2022).
39. E. Kyeyune-Nyombi *et al.*, High-resolution of particle contacts via fluorophore exclusion in deep-imaging of jammed colloidal packings. *Phys. A: Stat. Mech. Appl.* **490**, 1387–1395 (2018).
40. T. Aste, M. Saadatfar, T. J. Senden, Geometrical structure of disordered sphere packings. *Phys. Rev. E Stat. Nonlin. Soft Matter Phys.* **71**, 061302 (2005).
41. Y. Wang, Y. Wang, J. Zhang, Connecting shear localization with the long-range correlated polarized stress fields in granular materials. *Nat. Commun.* **11**, 4349 (2020).
42. J. N. Nampoothiri *et al.*, Emergent elasticity in amorphous solids. *Phys. Rev. Lett.* **125**, 118002 (2020).
43. C. Scalliet, L. Berthier, F. Zamponi, Absence of marginal stability in a structural glass. *Phys. Rev. Lett.* **119**, 205501 (2017).
44. S. Albert, G. Biroli, F. Ladieu, R. Tourbot, P. Urbani, Searching for the Gardner transition in glassy glycerol. *Phys. Rev. Lett.* **126**, 028001 (2021).
45. P. Rissone, E. I. Corwin, G. Parisi, Long-range anomalous decay of the correlation in jammed packings. *Phys. Rev. Lett.* **127**, 038001 (2021).
46. S. Wilken, R. E. Guerra, D. J. Pine, P. M. Chaikin, Hyperuniform structures formed by shearing colloidal suspensions. *Phys. Rev. Lett.* **125**, 148001 (2020).
47. S. Wilken, R. E. Guerra, D. Levine, P. M. Chaikin, Random close packing as a dynamical phase transition. *Phys. Rev. Lett.* **127**, 038002 (2021).
48. C. E. Zachary, Y. Jiao, S. Torquato, Hyperuniform long-range correlations are a signature of disordered jammed hard-particle packings. *Phys. Rev. Lett.* **106**, 178001 (2011).
49. D. Hexner, P. Urbani, F. Zamponi, Can a large packing be assembled from smaller ones? *Phys. Rev. Lett.* **123**, 068003 (2019).
50. C. Brito, H. Ikeda, P. Urbani, M. Wyart, F. Zamponi, Universality of jamming of nonspherical particles. *Proc. Natl. Acad. Sci. U.S.A.* **115**, 11736–11741 (2018).